Since January 2020 Elsevier has created a COVID-19 resource centre with free information in English and Mandarin on the novel coronavirus COVID-19. The COVID-19 resource centre is hosted on Elsevier Connect, the company's public news and information website.

Cell Reports

Article

Follicular T cells optimize the germinal center response to SARS-CoV-2 protein vaccination in mice

Graphical abstract

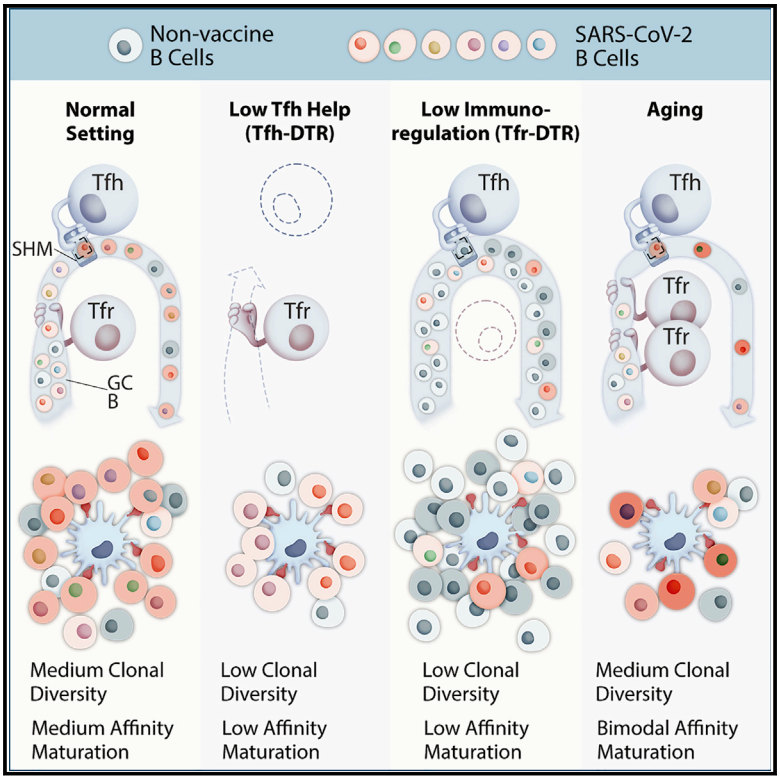

Highlights

- Tfh and Tfr cells are required for affinity maturation of GC B cells
- Tfh and Tfr cells optimize antibody responses to SARS-CoV-2 vaccines
- Aged mice have defective GC responses leading to bimodal antibody responses
- Tfh/Tfr help balance affinity maturation with clonal diversity in germinal centers

Authors

Cecilia B. Cavazzoni, Benjamin L. Hanson, Manuel A. Podestà, ..., Rob C. Oslund, Daria J. Hazuda, Peter T. Sage

Correspondence

psage@bwh.harvard.edu

In brief

Cavazzoni et al. show that both Tfh and Tfr cells are essential for optimization of germinal center responses to SARS-CoV-2 vaccines. Limiting Tfh cells results in fewer SARS-CoV-2 GC responses and lower affinity maturation, whereas limiting Tfr cells promotes non-antigen-specific GC responses, leading to lower-affinity maturation. Altered Tfh/Tfr responses in aging result in unique bimodal antibody responses.

Cavazzoni et al., 2022, Cell Reports *38*, 110399
February 22, 2022
https://doi.org/10.1016/j.celrep.2022.110399

CellPress

Cell Reports

CellPress
OPEN ACCESS

Article

Follicular T cells optimize the germinal center response to SARS-CoV-2 protein vaccination in mice

Cecilia B. Cavazzoni,[1] Benjamin L. Hanson,[1] Manuel A. Podestà,[1,2] Elsa D. Bechu,[1] Rachel L. Clement,[1] Hengcheng Zhang,[1] Joe Daccache,[1] Tamara Reyes-Robles,[3] Erik C. Hett,[3] Kalpit A. Vora,[3,4] Olugbeminiyi O. Fadeyi,[3] Rob C. Oslund,[3] Daria J. Hazuda,[3,4] and Peter T. Sage[1,5,*]

[1]Transplantation Research Center, Renal Division, Brigham and Women's Hospital, Harvard Medical School, Boston, MA 02115, USA
[2]Renal Division, Department of Health Sciences, Università degli Studi di Milano, Milano, Italy
[3]Merck Exploratory Science Center, Merck & Co., Inc., Cambridge, MA 02141, USA
[4]Department of Infectious Diseases and Vaccines Research, Merck & Co., Inc., West Point, PA, USA
[5]Lead contact
*Correspondence: psage@bwh.harvard.edu
https://doi.org/10.1016/j.celrep.2022.110399

SUMMARY

Follicular helper T (Tfh) cells promote, whereas follicular regulatory T (Tfr) cells restrain, germinal center (GC) reactions. However, the precise roles of these cells in the complex GC reaction remain poorly understood. Here, we perturb Tfh or Tfr cells after SARS-CoV-2 spike protein vaccination in mice. We find that Tfh cells promote the frequency and somatic hypermutation (SHM) of Spike-specific GC B cells and regulate clonal diversity. Tfr cells similarly control SHM and clonal diversity in the GC but do so by limiting clonal competition. In addition, deletion of Tfh or Tfr cells during primary vaccination results in changes in SHM after vaccine boosting. Aged mice, which have altered Tfh and Tfr cells, have lower GC responses, presenting a bimodal distribution of SHM. Together, these data demonstrate that GC responses to SARS-CoV-2 spike protein vaccines require a fine balance of positive and negative follicular T cell help to optimize humoral immunity.

INTRODUCTION

High-affinity antibodies are thought to be a direct result of the germinal center (GC) reaction, which promotes somatic hypermutation (SHM) and affinity maturation (Victora and Nussenzweig, 2012; Mcheyzer-Williams et al., 2012). Class-switch recombination (CSR) has also been attributed to the GC reaction, although CSR may be induced before B cells enter GCs (Roco et al., 2019). Follicular helper T (Tfh) cells are essential for GC responses because they provide cytokine and costimulatory signals (Crotty, 2019). Patients with mutations in Tfh effector molecules develop a primary immunodeficiency-like disease (Tangye et al., 2013; Kotlarz et al., 2014). Limited Tfh help has been thought to promote affinity maturation and clonal expansion through competition between B cells in the GC (Crotty, 2019). In support of this, enhancing Tfh-B interactions by targeting antigens to B cells promotes dark-zone cycling and clonal expansion (Victora et al., 2010; Gitlin et al., 2015). However, enhanced Tfh-B interactions may have positive or negative effects on selection of high-affinity clones (Victora et al., 2010; Gitlin et al., 2015). Moreover, induction of metabolic flux in B cells results in diminished affinity maturation (Ersching et al., 2017). However, untangling the roles of Tfh help from enhanced antigenic signals into B cells in these systems is difficult. Using an alternative strategy of reduced major histocompatibility complex (MHC) expression on B cells, a recent study showed that the peptide:MHC concentration controls GC entry, but not affinity maturation (Yeh et al., 2018). The precise roles of Tfh cells in optimizing GC responses remain poorly understood.

B cell responses can be fine-tuned by regulatory mechanisms in a process called humoral immunoregulation. Follicular regulatory T (Tfr) cells can gain access to the B cell follicle and restrain B cell responses (Sage and Sharpe, 2020; Fonseca et al., 2019; Wing et al., 2020). Alterations in Tfr cells have been associated with autoimmune disease and contribute to age-related defects in vaccination (Sage and Sharpe, 2020). Using a Tfr-deleter strategy, we showed that deletion of Tfr cells early before GC formation led to enhanced GC expansion and augmentation of autoantibodies (Clement et al., 2019). Other studies in which Bcl6 is deleted from T regulatory (Treg) cells (including Tfr cells) have confirmed the role of Tfr cells in controlling autoantibodies (Gonzalez-Figueroa et al., 2021; Wu et al., 2016; Fu et al., 2018). However, these studies have also suggested subtle (or positive) roles for Tfr cells in foreign antibody responses (Lu et al., 2021; Gonzalez-Figueroa et al., 2021; Wu et al., 2016; Fu et al., 2018).

In settings of SARS-CoV-2 infection, the frequencies of some subsets of Tfh cells correlate with anti-SARS-CoV-2 antibody responses, and defects in Tfh cells may contribute to mortality (Juno et al., 2020; Kaneko et al., 2020; Zhang et al., 2021). Tfr cells inversely correlate with SARS-CoV-2 antibody during infection (Gong et al., 2020). However, the precise roles of Tfh and Tfr cells in controlling GC responses remain poorly understood. Understanding how Tfh and Tfr cells control complex GC dynamics is critical for the development of strategies to enhance

vaccine efficacy to SARS-CoV-2 and other emerging pathogens. To address these questions, we utilized recently developed Tfh and Tfr deleter mice as well as models of aging to alter levels of follicular T cells during SARS-CoV-2 spike protein vaccination. We also incorporated single GC B cell culture assays along with B cell receptor (BCR) sequencing to determine the consequences of altering follicular T cells at the GC level. We found that Tfh cells were required for optimal SARS-CoV-2 Spike-specific B cell presence in GCs and for SHM, but controlled clonal diversity. We also found that Tfr cells contributed to SARS-CoV-2 spike-specific GC frequencies and promoted SHM and expansion of Spike-specific clones. Although Tfh and Tfr cells are classically thought of as stimulatory and inhibitory mediators of vaccine responses, respectively, we posit that these cells have dynamic and complex roles in optimizing B cell responses.

RESULTS

SARS-CoV-2 Spike protein vaccination generates robust germinal center responses in mice

Tfh cells have been implicated as being essential for GC responses, although the distinct roles of Tfh cells in controlling GC dynamics in a polyclonal environment are poorly understood. Moreover, Tfh (and Tfr) cell frequencies have been linked to SARS-CoV-2 antibody responses (Kaneko et al., 2020; Juno et al., 2020; Zhang et al., 2021). To understand follicular T cell and GC responses in more detail in the context of SARS-CoV-2 vaccination, we vaccinated wild-type mice with a SARS-CoV-2 prefusion Spike trimer using AddaVax as an adjuvant and harvested the draining lymph nodes (dLN). We found an increase in the total follicular T cell population whether we identified follicular T cells as $CD4^+ICOS^+CXCR5^+$ or $CD4^+PD\text{-}1^{hi}CXCR5^+$ cells, the latter likely indicating a "GC-like" phenotype (Figure 1A). We subdivided total follicular T cells ($CD4^+PD\text{-}1^{hi}CXCR5^+CD19^-$) into $FoxP3^-$ Tfh cells and $FoxP3^+$ Tfr cells and found that Tfh cells expanded after vaccination, whereas Tfr cells did not change (Figure 1B). This made the Tfr percentage of all follicular T cells lower compared with control non-vaccinated mice, although this did not reach statistical significance. $FAS^+GL7^+CD19^+$ GC B cells and $IgG1^+CD38^-$ class-switched B cells were substantially increased in the dLN compared with unvaccinated mice (Figures 1C and 1D). The SARS-CoV-2 vaccine also generated serological IgG responses to the S1, receptor binding domain (RBD), and S2 domains of SARS-CoV-2 Spike (Figure 1E). To understand the specificity of GC B cells in these settings, we used a single GC B cell culture assay to investigate the specificity, affinity, and BCR sequence of GC B cells at the single-cell (e.g., clonal) level (Kuraoka et al., 2016). These assays are advantageous because specificity can be obtained through sensitive ELISA rather than antigen probes, which may detect only high-affinity clones. Using this assay, we cultured individual GC B cells from mice immunized with the SARS-CoV-2 vaccine 14 days prior. Day 14 corresponds to the peak of the GC response (Figure S1). Presence of IgG was screened by ELISA, and IgG^+ wells were assessed for SARS-CoV-2 Spike reactivity. We found that ~24% of IgG^+ GC B cells were specific for SARS-CoV-2 Spike (Figures 1F and 1G). These data demonstrate that a SARS-CoV-2 Spike protein vaccine can generate Tfh cells as well as robust Spike-specific GC responses.

Tfh cells optimize early SARS-CoV-2-specific germinal center responses after protein vaccination

The precise roles of Tfh cells in mediating clonal dynamics within GCs have remained poorly understood due to a lack of tools. We recently developed a "Tfh-DTR" mouse to delete Tfh cells with administration of diphtheria toxin (DT) (Mohammed et al., 2021). The Tfh-DTR contains both $Cd4^{Cre}$ and $Cxcr5^{LoxSTOPLoxDTR}$ alleles, which posits the DT receptor (DTR) on the surface of $CD4^+$ T cells expressing CXCR5, including Tfh cells. Tfr cells will also be deleted in the Tfh-DTR mouse, but we refer to it as the Tfh-DTR for simplicity (Mohammed et al., 2021). We vaccinated control ($Cd4^{Cre}Cxcr5^{wt}$) or Tfh-DTR ($Cd4^{Cre}$ $Cxcr5^{LoxSTOPLoxDTR}$) mice with the SARS-CoV-2 Spike protein vaccine, administered DT, and assessed responses on day 14. The dLN from control mice contained $CD4^+PD\text{-}1^+CXCR5^+$ follicular T cells, which were almost completely missing from Tfh-DTR mice (Figure 2A). Deletion was specific for follicular T cells and was equally robust for Tfh and Tfr cells (Figures 2A and 2B). The frequency of GC B cells was diminished by ~50% in Tfh-DTR mice, indicating that Tfh cells are essential for robust GC responses (Figure 2C). At this early time point we did not find alterations in the concentration of Spike-specific IgG in serum, although RBD-specific IgG was slightly attenuated (Figures 2D and S1A).

To assess how Tfh cells control GC responses in more detail, we vaccinated control or Tfh-DTR mice, deleted Tfh cells, and, on day 14, performed single GC B cell culture assays. We screened cultures for presence of IgG and then Spike reactivity (Figure 2E). We found that in control mice 42.85% of IgG^+ GC B cells were specific for SARS-CoV-2 Spike. In contrast, only 11.63% of IgG^+ GC B cells were specific for Spike in Tfh-deleted mice (Figures 2E–2G). These data suggest Tfh cells may be required for Spike-specific B cell entry into GCs, although altered survival and proliferation are also likely factors. Moreover, some GC B cell clones from Tfh-DTR mice showed evidence of lower affinity (i.e., higher K_D values) (Figure 2F). To assess whether Tfh cells are required for SHM we performed similar experiments in which control or Tfh-DTR mice were vaccinated and single GC B cells were sorted at day 14 and immediately processed for BCR sequencing. When we assessed the total number of mutations in Vh segments we found no substantial differences between control or Tfh-DTR mice (Figures 2H and S1B). However, when we subdivided clones (defined as same V-J, CDR-H3 length, and at least 80% identity of amino acid sequence) based on the extent of expansion, we found that expanded clones in control mice had increased mutations compared with singletons, which was not found in Tfh-DTR mice (Figure 2I). In particular, highly expanded clones (found four or more times) had lower SHM in Tfh-DTR compared with control mice. These data suggest that Tfh cells are required for SHM during clonal expansion of B cells within GCs. We also assessed the extent of clonal expansion. We found that control mice had some evidence of clonal expansion, including an RBD-specific clone (VH2-9-1/JH4) found in a previous study (Alsoussi et al., 2020) (Figure 2J). Additional SARS-CoV-2

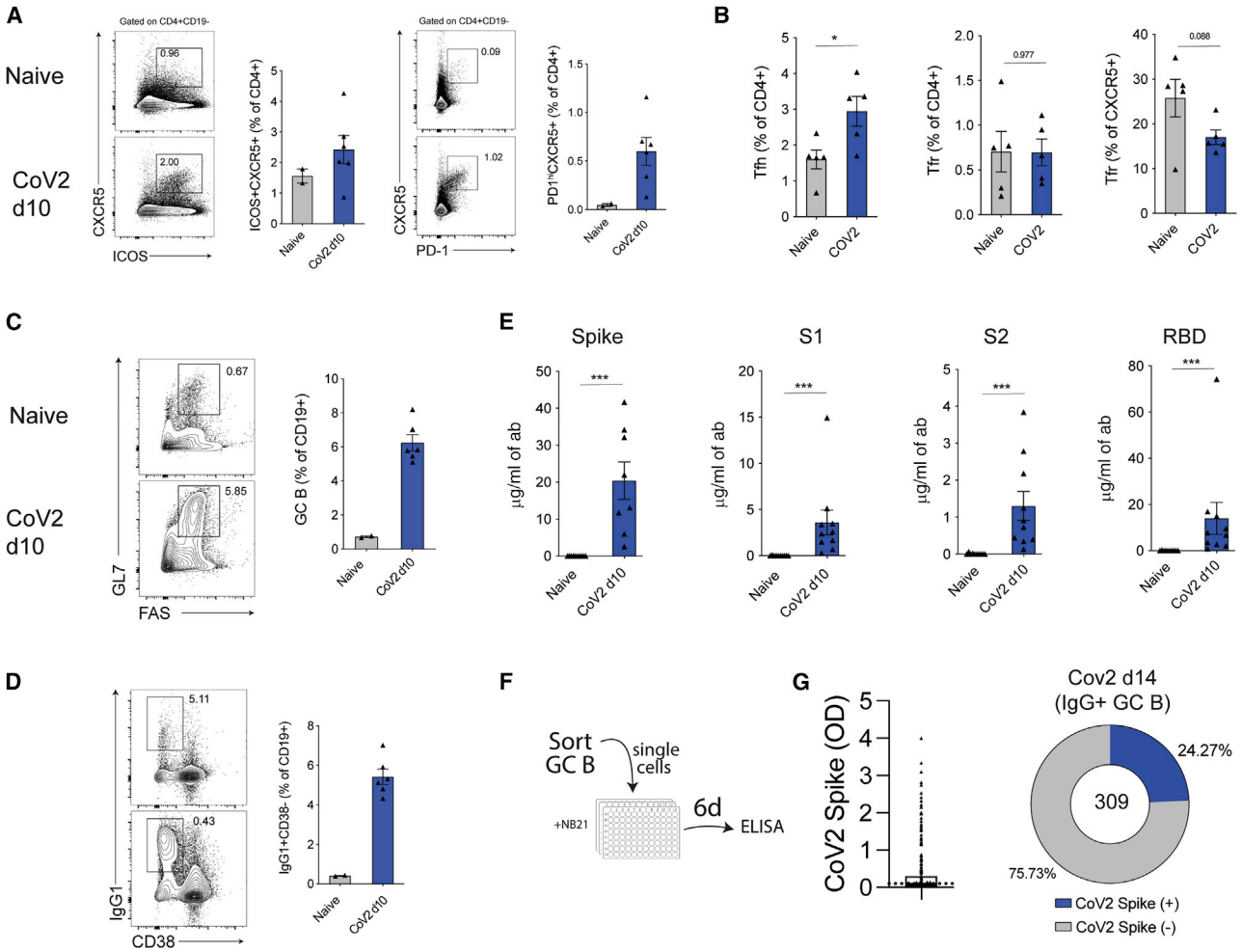

Figure 1. An adjuvanted SARS-CoV-2 subunit vaccine generates germinal center responses

(A) Frequency of follicular T cells identified as $CD4^+ICOS^+CXCR5^+$ (left) or $CD4^+PD\text{-}1^{hi}CXCR5^+$ (right) cells from the draining lymph node of naive mice or mice vaccinated with adjuvanted SARS-CoV-2 Spike protein vaccine 10 days prior.

(B) Frequencies of Tfh and Tfr cells as a percentage of total $CD4^+$ T cells (left and middle) or Tfr cells as a percentage of total follicular T ($CD4^+CXCR5^+PD1^+$) cells (right).

(C and D) Percentage of $CD19^+GL7^+FAS^+$ GC B cells (C) or $CD19^+IgG1^+CD38^-$ class-switched B cells (D) as a percentage of all $CD19^+$ B cells.

(E) Serological assessment of IgG for SARS-CoV-2 Spike, S1, S2, or RBD domains 10 days after vaccination.

(F) Schematic of single GC B cell culture assays. Single GC B cells from mice vaccinated with SARS-CoV-2 vaccine 14 days prior were cultured with NB21 feeder cells for 6 days. Culture supernatants were screened for IgG positivity. IgG^+ wells were investigated for SARS-CoV-2 Spike specificity.

(G) Distribution of SARS-CoV-2 Spike specificity from IgG^+ GC B cell cultures. Number in circle indicates total number of IgG^+ cells analyzed. Data are from a single experiment and are representative of three independent repeats (A–D), are combined data from three independent repeats with n = 2–6 mice per group (E), or are combined data of individual single GC B cell cultures taken from at least six independent repeats and are representative of n = 15 mice total (G). Student's two-tailed unpaired t test (A–E). ***$p < 0.001$ and *$p < 0.05$.

clones were annotated from our single GC B cell culture assays (Table S1). GC B cells from the Tfh-DTR mouse had more clonal expansion; some of which were identical in VH/JH segment usage, CDR-H3 length, and CDR-H3 amino acid sequence to Spike-specific clones. To assess clonal diversity, we calculated the N75 index using two different identity cutoffs for clonal assignment (Mesin et al., 2020)). An 80% identity cutoff identifies and groups clonotypes that potentially diverged from a common ancestor, whereas a 100% identity cutoff strictly discriminates between clonotypes. We found that Tfh-DTR mice had a lower N75 index at both 100% and 80% identity, indicating less clonal diversity compared with control mice. Since we found lower frequencies of Spike-specific B cells (as determined by culture assays), but also less clonal diversity (as determined by *ex vivo* BCR sequencing) in GCs, these data suggest that, in the absence of Tfh cells, there are fewer Spike-specific B cell clones in GCs, but these clones are able to expand to a greater extent. Therefore, Tfh cells promote the presence and SHM of SARS-CoV-2 Spike B cells in GCs but also promote clonal diversity.

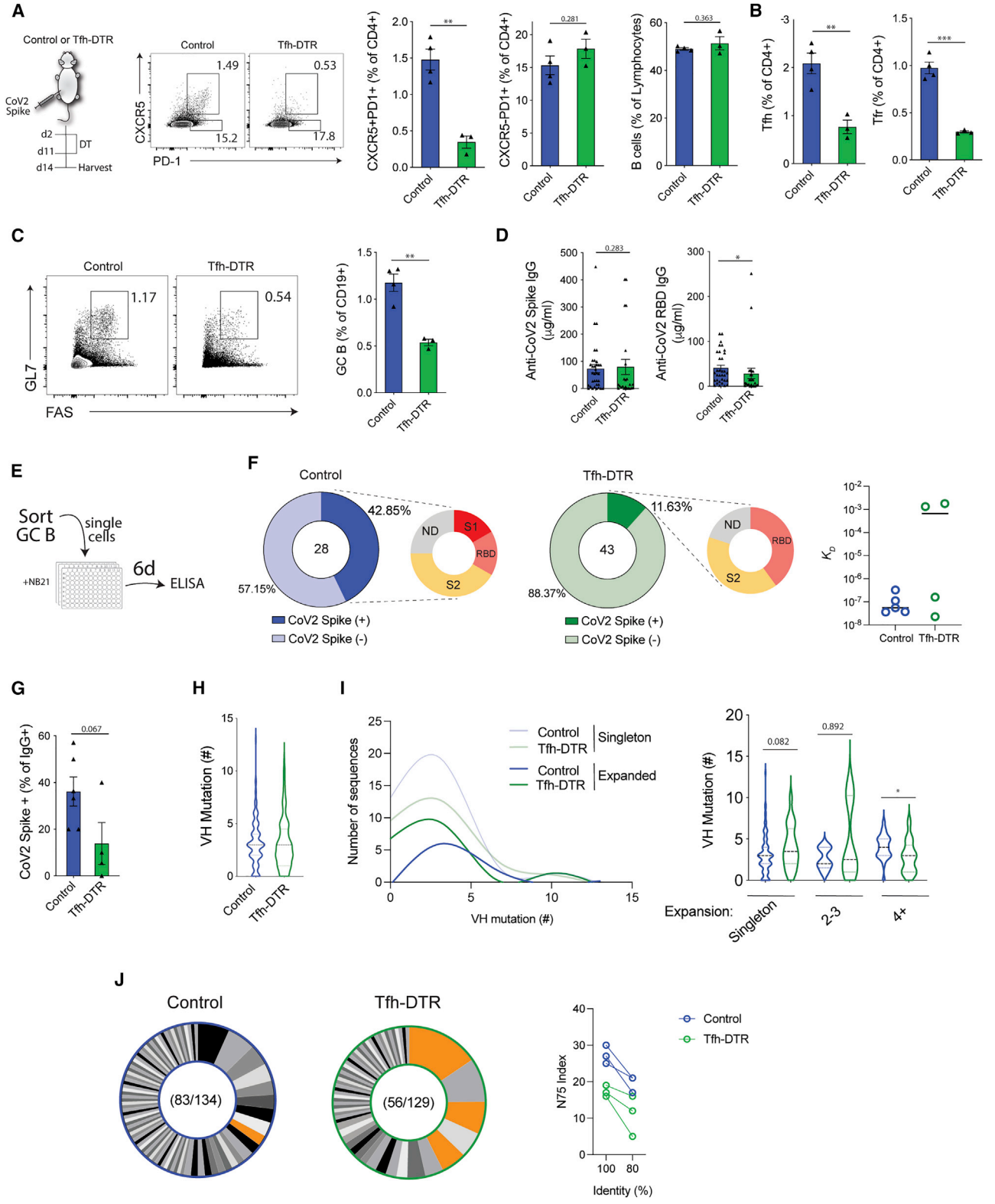

(legend on next page)

Tfr cells promote SARS-CoV-2-specific GC responses by limiting competition after vaccination

The role of Tfr cells in controlling GC responses to foreign antigens has remained controversial, with some studies finding that Tfr cells limit, whereas others promote, GC B cells (Sage and Sharpe, 2020). To study the role of Tfr cells in regulating GC clonal dynamics, we used Tfr-DTR mice, which allows deletion of Tfr cells with DT (Clement et al., 2019; Mohammed et al., 2021). We vaccinated control (*Foxp3*^{Cre} *Cxcr5*^{wt}) or Tfr-DTR (*Foxp3*^{Cre} *Cxcr5*^{LoxSTOPLoxDTR}) mice with the SARS-CoV-2 Spike protein vaccine and administered DT to delete Tfr cells. DT administration resulted in a severely attenuated frequency of Tfr cells but normal frequencies of Tfh, CXCR5^{-}PD1^{+}FoxP3^{-} T conventional cells, CXCR5^{-}PD1^{+}FoxP3^{+} Treg cells, and B cells (Figures 3A and 3B). We found an ~1.5-fold increase in the frequency of GC B cells and an ~2-fold increase in IgG1^{+}CD38^{-} class-switched B cells in Tfr-DTR, compared with control mice (Figures 3C and 3D). We did not find substantial differences in anti-SARS-CoV-2 Spike IgG, but did find slightly elevated anti-SARS-CoV-2 RBD IgG in sera (Figures 3E and S2A).

To study how Tfr regulation alters the clonal dynamics of SARS-CoV-2 Spike protein-specific B cell responses in GCs, we performed single GC B cell culture assays. We found that ~25% of IgG^{+} GC B cell clones from control mice were SARS-CoV-2 Spike specific, with almost half being specific for potentially neutralizing (S1 and RBD) epitopes (Figure 3F). In contrast, in Tfr-DTR mice only ~12% of GC B cells were specific for SARS-CoV-2 Spike, and of those cells, only a small fraction were specific for S1 and RBD (Figure 3F). Interestingly, roughly half of the SARS-CoV-2 Spike-specific GC B cells in Tfr-DTR mice did not have detectable reactivity to RBD, S1, or S2. It is possible that these cells are specific for conformational epitopes in the Spike trimer. We did not find any substantial reactivity of the clones to autoantigens (Figure S2B). When we assessed Spike-specific clones for affinity, we found lower affinities in Tfr-DTR mice (Figure 3G). These data suggest that, despite Tfr cells restraining GC B cell differentiation, they promote the relative abundance of vaccine-specific B cells in the GC reaction, most likely by limiting clonal competition. To determine how Tfr cells alter SHM of GC B cells, we performed BCR sequencing on total GC B cells sorted *ex vivo*. We did not find significant differences in the total number of mutations in GC B cells from control or Tfr-DTR mice (Figure 3H). However, when we separated the cells based on clonal expansion, we found that expanded clones in Tfr-DTR mice had fewer mutations compared with control mice with many germline sequences (Figures 3H and S2C). The most expanded clone in Tfr-DTR mice acquired few mutations and was found in two separate mice. Although clonality may skew mutational analyses, we found multiple clones in the 4+ category in Tfr-DTR mice. When we assessed clonal diversity, we found lower diversity in some Tfr-DTR mice (using 100% identity cutoff) (Figure 3I). However, the difference in diversity was less substantial using an 80% cutoff ($p = 0.397$ versus $p = 0.0735$ at 100% identity). Interestingly, we did not find any Spike-specific clones in Tfr-DTR mice based on sequence, but found some in control mice. Taken together, these data indicate that Tfr cells disproportionately restrain non-vaccine-specific GC B cells compared with SARS-CoV-2 clones, and that by limiting the total number of clones within the GC, Tfr cells are able to promote SHM and affinity maturation of Spike-specific B cells.

Age-associated humoral immunoregulation alters SARS-CoV-2 GC responses after vaccination

Many classical vaccination strategies have diminished effectiveness in the elderly due to age-related changes in the immune system. These changes include altered/defective Tfh cells and expansion of fully suppressive Tfr cells (Sage et al., 2015; Webb et al., 2021; Lefebvre et al., 2016). To understand how aging alters SARS-CoV-2 Spike-specific GC responses, we vaccinated 8-week-old "young" and 80-week-old "aged" mice with our adjuvanted SARS-CoV-2 Spike protein vaccine. On day 14 after vaccination, we found that aged mice had substantial increases in frequencies of Tfh and Tfr cells (Figures 4A and S3A). We found evidence that Tfh cells were responding to antigen in aged mice because they expressed the cell-cycle marker Ki67+ (Figure S3B). We also found increased frequencies of CXCR5^{-}FoxP3^{+} Treg cells and total CD19^{+} B cells (Figure 4B).

Figure 2. Tfh cells optimize early SARS-CoV-2 Spike-specific germinal center responses after adjuvanted protein vaccination

(A) Assessment of total CD4^{+}PD-1^{+}CXCR5^{+} follicular T cells (left), CD4^{+}PD-1^{+}CXCR5^{-} T cells (middle), and CD19^{+} B cells (right) from draining lymph nodes of control (*Cd4*^{Cre} *Cxcr5*^{wt}) or Tfh-DTR (*Cd4*^{Cre} *Cxcr5*^{LoxSTOPLoxDTR}) mice that were vaccinated with an adjuvanted SARS-CoV-2 Spike protein vaccine, given DT, and harvested on day 14.

(B) Frequencies of CD4^{+}PD-1^{+}CXCR5^{+}FoxP3^{-} Tfh (left) and CD4^{+}PD-1^{+}CXCR5^{+}FoxP3^{+} Tfr (right) cells.

(C) Percentage of CD19^{+}GL7^{+}FAS^{+} GC B cells out of all CD19^{+} B cells.

(D) Serological assessment of SARS-CoV-2 Spike and RBD-specific IgG from serum of vaccinated mice.

(E) Schematic for single GC B cell cultures.

(F) Assessment of SARS-CoV-2 Spike specificity for IgG^{+} GC B cells using single GC culture assays. Numbers in circles indicate total number of IgG^{+} GC B cells analyzed. ND, not determined to be specific for S1, RBD, or S2; S1, specific for S1 but not RBD; RBD, specific for RBD; S2, specific for S2. K_D indicates equilibrium dissociation constant for Spike-specific B cell clones measured by biolayer interferometry.

(G) Assessment of SARS-CoV-2 Spike-specific IgG^{+} GC B cells using single GC culture assays separated by individual mice.

(H) BCR somatic hypermutation analysis for V-heavy (VH) chain in *ex vivo* sorted GC B cells.

(I) Mutation analysis for singleton and expanded (found at least twice) clones using smoothing spline fitting of data.

(J) Analysis of clonal distribution from *ex vivo* GC B cells. Numbers indicate total number of clones and number of GC B cells analyzed. Orange indicates Spike specificity from published or single-cell GC B cell culture sequences. N75 index indicates the smallest number of clones to comprise 75% of sequenced cells and is represented on a per-mouse basis. Data are from a single experiment and are representative of three independent repeats with n = 3–4 mice per group (A–C, F), are concatenated data from two independent experiments with n = 6–12 mice per group (D), are concatenated data from two independent experiments (G), or are concatenated data from n = 3 mice per group from one experiment (H–J). Student's two-tailed unpaired t test (A–F) or Mann-Whitney test (I). ***$p < 0.001$, **$p < 0.01$, *$p < 0.05$. See also Figure S1.

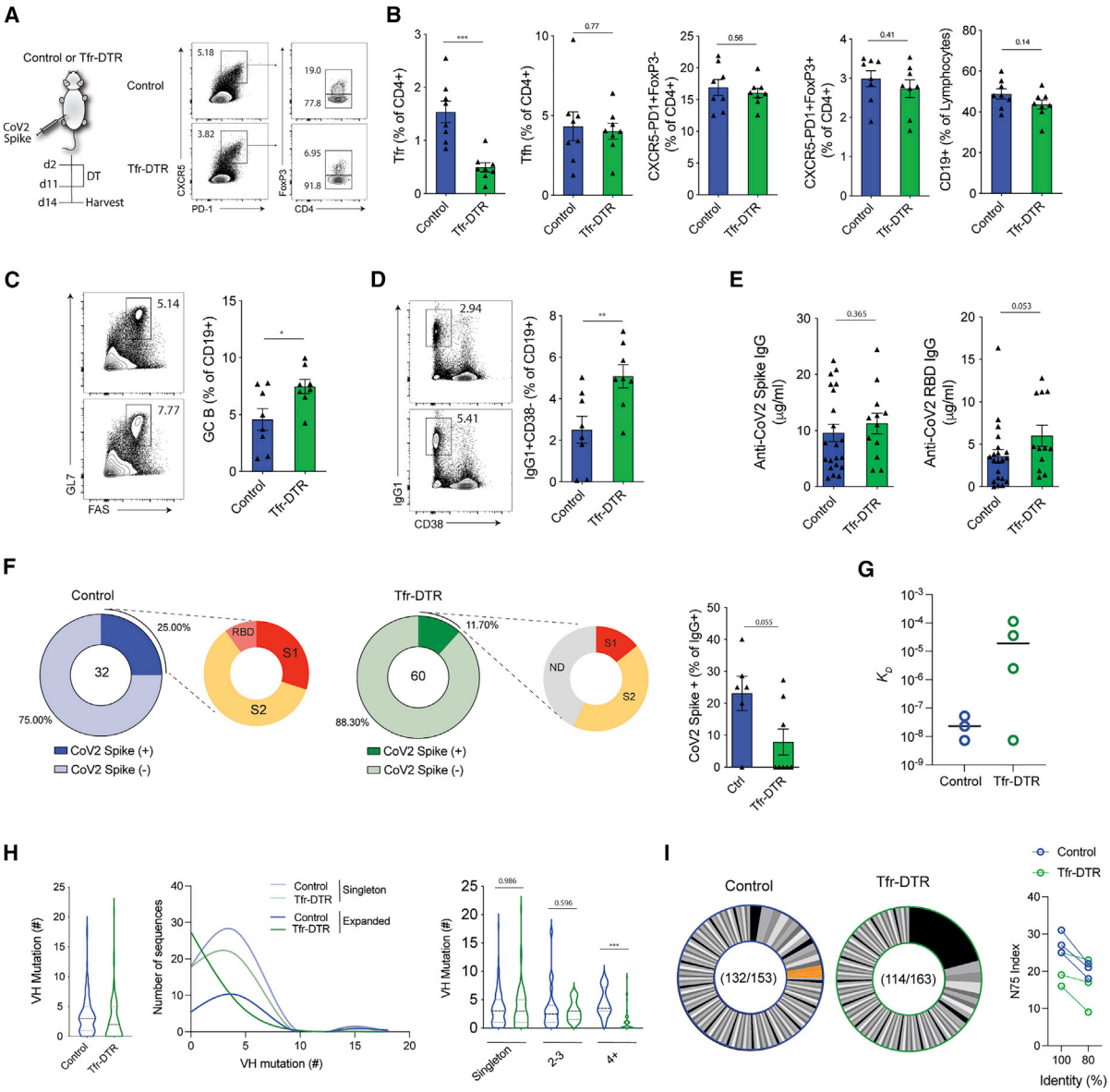

Figure 3. Tfr cells promote SARS-CoV-2 Spike-specific GC responses by limiting competition after vaccination

(A) Assessment of total $CD4^+PD\text{-}1^+CXCR5^+$ follicular T cells (right) from draining lymph nodes of control (*Foxp3*^{Cre} and *Cxcr5*^{wt}) or Tfr-DTR (*Foxp3*^{Cre} *Cxcr5*^{LoxSTOPLoxDTR}) mice that were vaccinated with an adjuvanted SARS-CoV-2 Spike-protein vaccine, given DT, and harvested on day 14.

(B) Frequencies of $CD4^+PD\text{-}1^+CXCR5^+FoxP3^+$ Tfr, $CD4^+PD\text{-}1^+CXCR5^+FoxP3^-$ Tfh, $CD4^+PD\text{-}1^+CXCR5^-FoxP3^-$ T cells, $CD4^+PD\text{-}1^+CXCR5^+FoxP3^+$ Treg cells, and $CD19^+$ B cells.

(C) Percentage of $CD19^+GL7^+FAS^+$ GC B cells out of all $CD19^+$ B cells.

(D) Percentage of $CD19^+IgG1^+CD38^-$ class-switched B cells as a percentage of all $CD19^+$ B cells.

(E) Serological analysis of SARS-CoV-2 Spike or RBD-specific IgG.

(F) Percentage of SARS-CoV-2 Spike-specific clones as a percentage of IgG^+ GC B cells from single-cell GC cultures, along with individual epitope specificity. Number in the center of the circle plot indicates total number of IgG^+ GC B cells analyzed. ND, not determined to be specific for S1, RBD, or S2; S1, specific for S1 but not RBD; RBD, specific for RBD; S2, specific for S2. (Right) Percentage of SARS-CoV-2 Spike-specific cells as a percentage of IgG^+ GC B cells from individual mice.

(G) Affinities of Spike-specific antibodies from (F).

(H) BCR somatic hypermutation analysis for V-heavy (VH) chain in *ex vivo* sorted GC B cells, including analysis for singleton and expanded (found at least twice) clones using smoothing spline fitting of data.

(I) Analysis of clonal distribution and diversity from *ex vivo* GC B cells. Numbers indicate total number of clones and number of GC B cells analyzed. N75 index is represented on a per-mouse basis. Data are from a single experiment and are representative of three independent repeats with n = 4–8 mice per group (A–D), are concatenated data from two independent experiments with at least six mice per group (E), are concatenated data from two independent experiments (F and G), or are concatenated data from n = 3 mice per group from one experiment (H and I). Student's two-tailed unpaired t test (A–G) or Mann-Whitney test (H). ***$p < 0.001$, **$p < 0.01$, *$p < 0.05$. See also Figure S2.

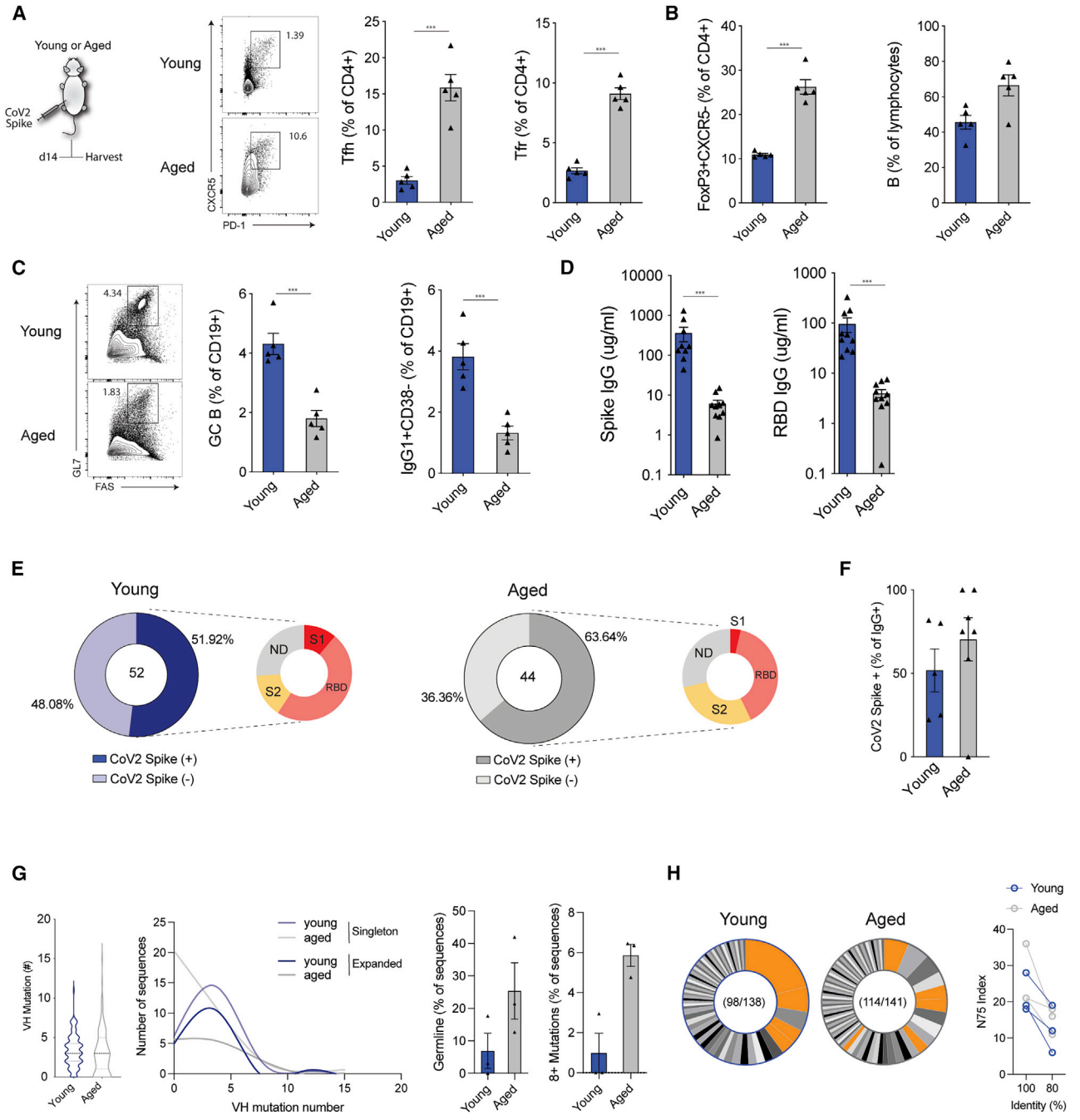

Figure 4. Age-associated humoral immunoregulation alters SARS-CoV-2 GC responses after Spike protein vaccination

(A) Assessment of total $CD4^+PD\text{-}1^+CXCR5^+$ follicular T (left), $CD4^+PD\text{-}1^+CXCR5^+FoxP3^-$ Tfh (middle), and $CD4^+PD\text{-}1^+CXCR5^+FoxP3^+$ Tfr (right) cells from draining lymph nodes of young (8 weeks old) or aged (80 weeks old) mice that were vaccinated with an adjuvanted SARS-CoV-2 Spike protein vaccine and harvested on day 14.

(B) Percentage of $CD4^+FoxP3^+CXCR5^-$ Treg cells (left) and total $CD19^+$ B lymphocytes (right).

(C) Percentage of $CD19^+GL7^+FAS^+$ GC B cells out of all $CD19^+$ B cells (left) and $CD19^+IgG1^+CD38^-$ class-switched B cells as a percentage of all $CD19^+$ B cells (right).

(D) Serological analysis of SARS-CoV-2 Spike or RBD-specific IgG.

(E) Percentage of SARS-CoV-2 Spike-specific clones as a percentage of total IgG^+ GC B cells from single-cell GC cultures (left). Number in the center of the circle plot indicates total number of IgG + GC B cells analyzed. ND, not determined to be specific for S1, RBD, or S2; S1, specific for S1 but not RBD; RBD, specific for RBD; S2, specific for S2.

(legend continued on next page)

We found a 2-fold decrease in the frequency of $CD19^+GL7^+FAS^+$ GC B cells as well as a similar reduction in the frequency of $IgG1^+CD38^-$ class-switched B cells in aged mice (Figures 4C and S3B). Moreover, we found profound reductions in SARS-CoV-2 Spike- and RBD-specific IgG in the serum of aged mice compared with young mice (Figure 4D). These data demonstrate reduced humoral immunity and GC responses in aged mice.

To determine how aging alters GC clonal dynamics, we performed single GC B cell cultures. We found that ~50% of IgG^+ GC B cells in young mice were specific for SARS-CoV-2 Spike (Figures 4E and 4F). Surprisingly, we found slightly increased frequencies of SARS-CoV-2 Spike-specific GC B cells in aged mice. These data suggest that increases in Tfr cells (and altered Tfh cells) during aging may contribute to diminished GC B cell frequencies overall, but may allow vaccine-specific GC B cell responses by limiting interclonal competition. Next, we assessed BCR repertoire analysis on total sorted single GC B cells. We did not find any substantial changes in total SHM in aged mice, although we did find a much broader and bimodal distribution of mutations with more germline sequences but also more highly mutated clones (Figures 4G and S3C). We also assessed the clonal diversity of GC B cells. Young mice had some clonal expansion, including clones specific for SARS-CoV-2 Spike protein (Figure 4H). We found that aged mice had similar clonal expansion and clonal diversity compared with young mice. Together, these data indicate that changes in Tfr and Tfh cells during aging alter GC optimization, resulting in a broader distribution of SHM without subsequent changes in clonal diversity.

Early Tfr humoral immunoregulation alters SARS-CoV-2 Spike protein germinal center responses after vaccine boosting

To determine if regulation of early GC responses by Tfr cells translated into alterations after secondary challenge, we used a vaccine boosting strategy. We vaccinated control (*Foxp3*^{Cre} *Cxcr5*^{wt}) or Tfr-DTR (*Foxp3*^{Cre} *Cxcr5*^{LoxSTOPLoxDTR}) mice with the SARS-CoV-2 Spike protein vaccine and administered DT only until day 11. We boosted the mice at day 30 with the same adjuvanted SARS-CoV-2 vaccine and assessed the mice 8 days later (day 38 since initial vaccination) (Figure 5A). This strategy allowed for absence of Tfr cells during priming but presence during boosting. We included adjuvant in the vaccine boost to generate robust secondary GCs and to maintain consistency in the vaccine formulation. The frequencies of Tfh and Tfr cells were similar between control and Tfr-DTR mice 8 days after vaccine boosting, suggesting the Tfr cells had successfully repopulated (Figure 5B). The frequencies of $CD19^+GL7^+FAS^+$ GC B cells and $IgG1^+CD38^-$ class-switched B cells were both slightly elevated in Tfr-DTR mice compared with control mice, although this did not reach statistical significance (Figures 5C and 5D). Vaccine boosting resulted in substantial increases in SARS-CoV-2 Spike- and RBD-specific antibodies in serum of control mice (Figure 5E). However, we did not find any consistent differences in the amount of SARS-CoV-2 IgG in serum between Tfr-DTR and control mice.

We performed single GC B cell culture assays with GC B cells from vaccine-boosted mice. We found that the frequency of SARS-CoV-2 Spike-specific GC B cells out of all IgG^+ GC B cells was slightly elevated in Tfr-DTR mice, but this did not reach statistical significance (Figures 5F and 5G). However, only ~1/4 of these Spike-specific GC B cells were directed toward S1/RBD, in contrast to control mice, in which ~1/2 of Spike-specific GC B cells showed binding to S1/RBD. When we measured the affinities of Spike-specific clones we found that clones from Tfr-DTR mice had overall similar affinities compared with those from control mice (Figure 5H). We assessed the clones for autoreactivity and found increased autoreactivity of clones in early Tfr-deleted mice, but this did not reach statistical significance (Figure S5A). We also performed *ex vivo* BCR sequencing to determine if SHM and clonal expansion differed between control and Tfr-DTR mice. We did not find substantial changes in the average number of VH mutations in control versus Tfr-DTR mice when we assessed all GC B cells (Figures 5I and S4B). However, when we separated cells based on extent of clonal expansion, we found lower mutations for both singletons and greatly expanded clones in Tfr-DTR compared with control mice. We also assessed clonal diversity but did not find substantial differences between control and Tfr-DTR mice (Figure 5J). Together these data indicate that early Tfr humoral immunoregulation during primary GCs can affect secondary GCs after vaccine boosting by optimizing SHM.

We also assessed the contribution of Tfr cells at the time of vaccine boosting to GC B cell responses in secondary GCs. We vaccinated control (*Foxp3*^{Cre} *Cxcr5*^{wt}) or Tfr-DTR (*Foxp3*^{Cre} *Cxcr5*^{LoxSTOPLoxDTR}) mice with the adjuvanted SARS-CoV-2 Spike protein vaccine and boosted on day 30. We then administered DT from day 30 until day 36 to delete Tfr cells only during vaccine boosting. We harvested dLNs and serum on day 38 (8 days after boost) (Figure 5K). We found minor increases in Spike-specific serum IgG in Tfr-deleted mice, but this did not reach statistical significance (Figure 5L). We also assessed Spike-specific IgG^+ GC B cells using our single GC B cell culture assays but found no substantial differences in the frequency of Spike-specific GC B cells (Figure 5M). These data indicate that the roles of Tfr cells in controlling clonal dynamics in primary GCs may not be the same in secondary GCs after vaccine boosting.

Early Tfh help promotes SARS-CoV-2 Spike-specific germinal center responses after vaccine boosting

Next, we determined if optimization of the GC reaction by Tfh cells early during primary GCs altered secondary GC responses

(F) Percentage of SARS-CoV-2 Spike-specific cells as a percentage of total IgG + GC B cells in individual mice.
(G) BCR somatic hypermutation analysis for V-heavy (VH) chain in *ex vivo* sorted GC B cells, including analysis for singleton and expanded (found at least twice) clones using smoothing spline fitting of data.
(H) Analysis of clonal distribution from *ex vivo* GC B cells. Numbers indicate total number of clones and number of GC B cells analyzed. N75 index is represented on a per-mouse basis. Data are from a single experiment and are representative of three independent repeats with n = 4–8 mice per group (A–C), are concatenated data from two independent experiments with n = 4–6 mice per group (D), are concatenated data from two independent experiments (E and F), or are concatenated data from n = 3 mice per group from one experiment (G and H). Student's two-tailed unpaired t test (A–D). ***$p < 0.001$. See also Figure S3.

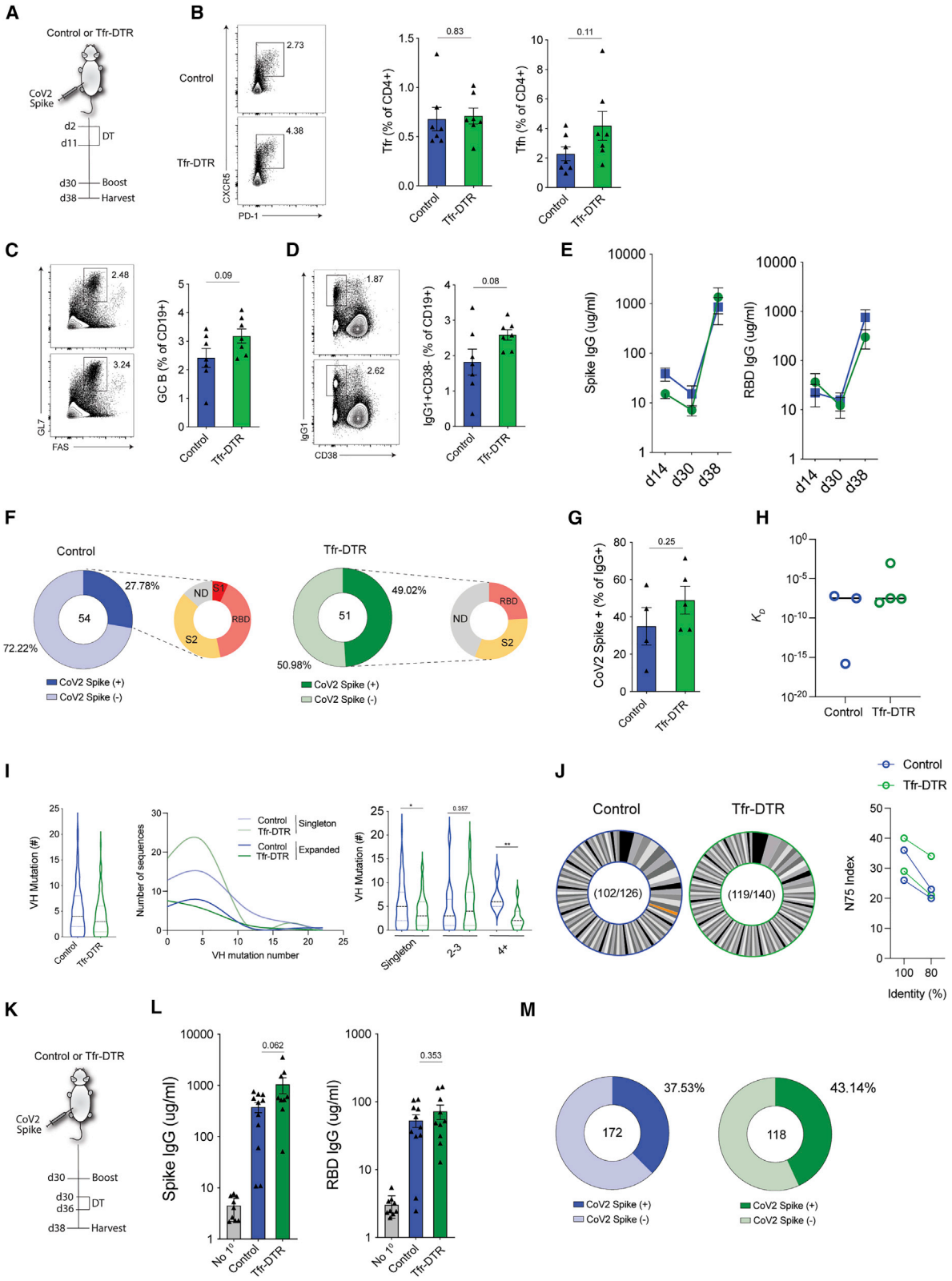

(legend on next page)

after vaccine boosting. To do this, we vaccinated control (*Cd4*^{Cre} and *Cxcr5*^{wt}) or Tfh-DTR (*Cd4*^{Cre} *Cxcr5*^{LoxSTOPLoxDTR}) mice with the adjuvanted SARS-CoV-2 recombinant Spike protein vaccine and administered DT only until day 11, boosted the mice with the same SARS-CoV-2 vaccine on day 30, and assessed dLNs on day 38 (Figure 6A). We found that Tfh cells had reconstituted by day 38, confirming the absence of Tfh cells only during primary responses (Figure 6B). However, Tfr cells were slightly attenuated at day 38. This difference likely reflects biological changes due to the loss of Tfh cells and not the lack of the ability of Tfr cells to reconstitute, because Tfr reconstitution in Tfr-DTR mice was complete with a similar deletion schedule. We found that GC B cell frequencies were similar between control and Tfh-DTR mice, suggesting no changes in GC B cell differentiation (Figure 6C). When we assessed SARS-CoV-2 Spike and RBD-specific IgG in serum, we found that boosting resulted in substantial increases in antibody responses that were comparable between control and Tfh-DTR mice (Figure 6D). These data demonstrate that early Tfh help in primary GCs does not affect GC B cell frequencies nor augmentation of serological antibody after secondary vaccination.

To understand how early Tfh help alters GC dynamics after secondary challenge we performed single GC B cell cultures. We found that ~23% of IgG$^+$ GC B cells were specific for SARS-CoV-2 Spike in control mice and ~17% in Tfh-DTR mice (Figure 6E). We found that antibodies produced by Spike-specific single GC B cell clones in Tfh-DTR mice had lower affinities than antibodies from control mice, although we were able to test only a few clones (Figure 6F). We also performed *ex vivo* single GC B cell *Igh* sequencing to assess SHM and clonal expansion. We found no difference in the number of mutations for IgM$^+$ antibodies but did find a reduced number of mutations in IgG$^+$ GC B cells in Tfh-DTR compared with control mice (Figures 6G and S5A). We further separated GC B cells based on expansion and found that non-expanded and greatly expanded (>4) clones had evidence of lower numbers of mutations in Tfh-DTR compared with control mice. We also assessed clonal expansion and clonal diversity and found similar distributions of clones in control and Tfh-DTR mice (Figure 6H). Together these data indicate that early Tfh help is important for optimal SHM and affinity maturation from secondary GCs after vaccine boosting.

We also performed experiments in which we deleted Tfh cells during vaccine boosting. We vaccinated control (*Cd4*^{Cre} and *Cxcr5*^{wt}) or Tfh-DTR (*Cd4*^{Cre} *Cxcr5*^{LoxSTOPLoxDTR}) mice with the adjuvanted SARS-CoV-2 Spike protein vaccine, and mice were boosted on day 30. After boosting, DT was administered to delete Tfh cells. We harvested dLNs and serum on day 38 (8 days after boost) (Figure 6I). We did not find any differences in Spike-specific nor RBD-specific serum antibody between control and Tfh-deleted mice (Figure 6J). To assess Spike-specific IgG$^+$ GC B cells, we performed single GC B cell cultures. We found that secondary GCs (at day 38) had slight increases in Spike-specific B cells when Tfh cells were deleted at the time of boosting. Nonetheless, both control and deleter mice presented higher frequency of Spike-specific GC B cells than controls at day 8 (given only one dose of the vaccine at day 30) (Figure 6K). This is in contrast to primary GCs, which showed decreases in Spike-specific GC B cells when Tfh cells were deleted. These studies suggest that Tfh cells may have different roles in optimizing Spike-specific GC B cells during primary and secondary GCs.

DISCUSSION

The role of Tfh cells in mediating the dynamics of the GC reaction has been studied previously by modulating antigen presentation of, or metabolic flux in, GC B cells. Although these alterations may be consistent with Tfh help, Tfh cells may alter GC responses through a number of mechanisms. Moreover, the role of Tfh cells in mediating GC clonal dynamics has remained controversial. More recently, a role for Tfh cells in GC contraction via upregulation of Foxp3 (and possibly by differentiating

Figure 5. Early Tfr humoral immunoregulation alters SARS-CoV-2 Spike-specific GC responses after vaccine boosting

(A) Schematic of experiment. Control (*Foxp3*^{Cre} and *Cxcr5*^{wt}) or Tfr-DTR (*Foxp3*^{Cre} *Cxcr5*^{LoxSTOPLoxDTR}) mice were vaccinated with an adjuvanted SARS-CoV-2 Spike protein vaccine and given DT until day 11. The mice received a SARS-CoV-2 vaccine boost on day 30 and draining lymph nodes were harvested on day 38.

(B) Assessment of total CD4$^+$PD-1$^+$CXCR5$^+$ follicular T (left), CD4$^+$PD-1$^+$CXCR5$^+$FoxP3$^+$ Tfr (middle), and CD4$^+$PD-1$^+$CXCR5$^+$FoxP3$^-$ Tfh (right) cells on day 38.

(C) Percentage of CD19$^+$GL7$^+$FAS$^+$ GC B cells out of all CD19$^+$ B cells.

(D) Percentage of CD19$^+$IgG1$^+$CD38$^-$ class-switched B cells out of all CD19$^+$ B cells.

(E) Serological analysis of SARS-CoV-2 Spike or RBD-specific IgG.

(F) Percentage of SARS-CoV-2 Spike-specific clones out of the total IgG$^+$ GC B cells from single-cell GC cultures. Number in the center of the circle plot indicates total number of IgG$^+$ GC B cells analyzed.

(G) Percentage of SARS-CoV-2 Spike-specific clones out of the total IgG$^+$ GC B cells in individual mice.

(H) Affinities of Spike-specific antibodies from single GC B cell cultures.

(I) BCR somatic hypermutation analysis for V-heavy (VH) chain in *ex vivo* sorted GC B cells, including analysis for singleton and expanded (found at least twice) clones using smoothing spline fitting of data.

(J) Analysis of clonal distribution and clonal diversity from *ex vivo* GC B cells. Numbers indicate total number of clones and number of GC B cells analyzed. N75 index is represented on a per-mouse basis.

(K) Schematic of deletion during boosting experiment. Control (*Foxp3*^{Cre} and *Cxcr5*^{wt}) or Tfr-DTR (*Foxp3*^{Cre} *Cxcr5*^{LoxSTOPLoxDTR}) mice were vaccinated with a SARS-CoV-2 Spike protein vaccine and were boosted on day 30 followed by DT treatment. Draining lymph nodes were harvested on day 38.

(L) Spike and RBD-specific IgG in serum from mice treated as in (K).

(M) Single GC B cell cultures from GC B cells as in (K). Numbers indicate total numbers of IgG$^+$ GC B cell clones analyzed. Data are from a single experiment and are representative of two independent repeats with n = 4–8 mice per group (A–D), are concatenated data from two independent experiments with n = 4–8 mice per group (E), are concatenated data from two independent experiments (E–H), are concatenated data from n = 3 mice per group from one experiment (I and J), or are concatenated data from two independent repeats with n = 4–6 mice per group (L and M). Student's two-tailed unpaired t test (A–E, I) or Mann-Whitney test (I). $^{**}p < 0.01$ and $^{*}p < 0.05$. See also Figure S4.

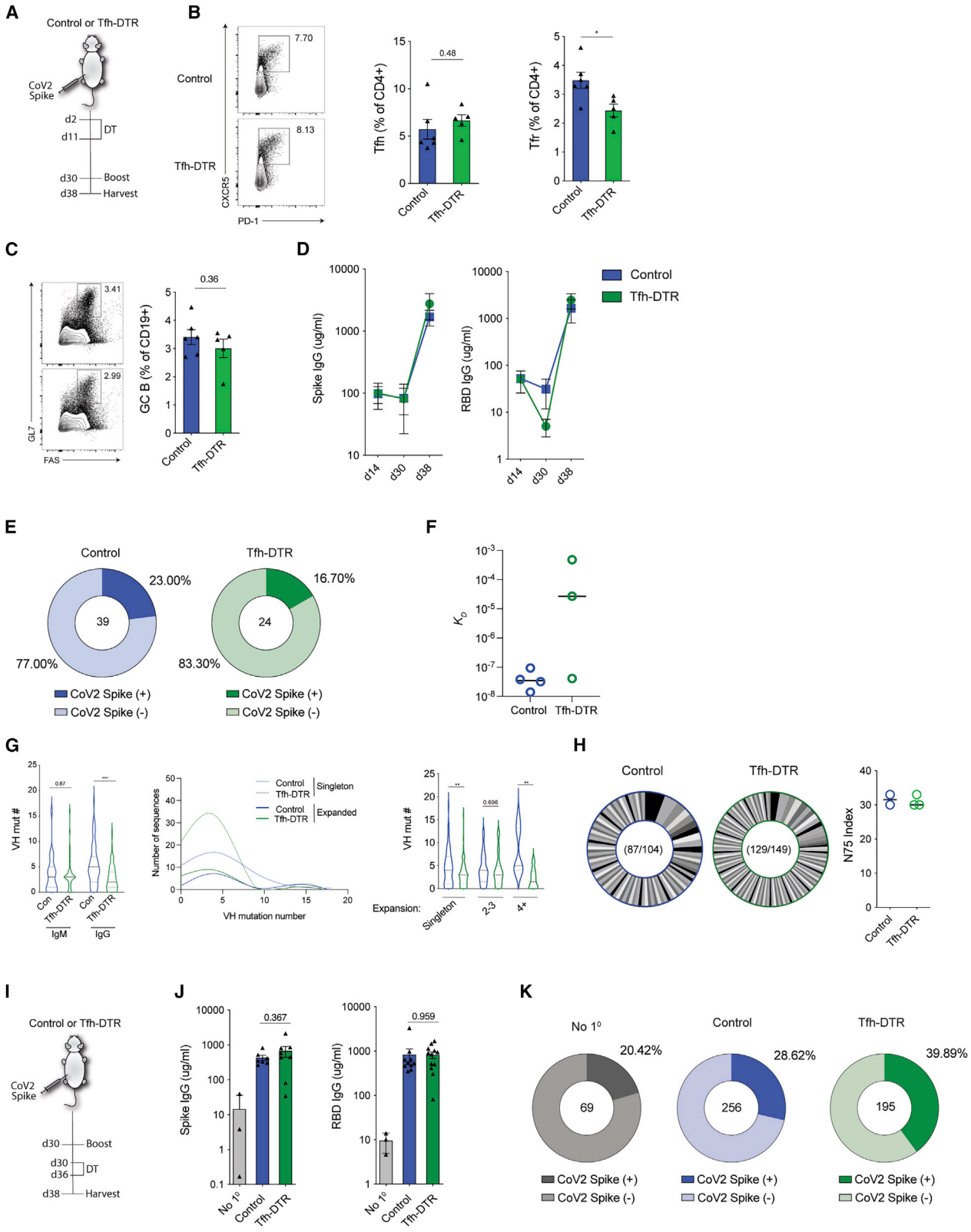

(legend on next page)

into Tfr-like cells) has also been described (Jacobsen et al., 2021). Therefore, we utilized a deletion strategy to largely eliminate Tfh cells at specific times. We found that Tfh cells promoted SHM in response to SARS-CoV-2 Spike protein vaccination. This was more evident in expanded clones, which is consistent with these clones receiving more stimulatory signals. Interestingly, the decrease in SHM when Tfh cells were deleted during primary vaccination persisted after vaccine boosting, even though Tfh cells have repopulated by this time. It is possible that the loss of Tfh cells during primary vaccination resulted in memory B cells with attenuated SHM that re-entered secondary GCs after vaccine boosting. This may partially explain the reduced SHM, since recent studies suggest that GC-experienced memory B cells account for only a small proportion of B cells in secondary GCs after vaccine boosting (Mesin et al., 2020). An alternative possibility is that the absence of Tfh cells during primary responses prevented memory Tfh cells from forming, and diminished SHM after boosting may be due to altered functionality between *de novo*-formed and memory-expanded Tfh cells. Moreover, the lack of Tfh help may have favored extrafollicular responses. Surprisingly, we found that Tfh cells simultaneously control diversity and clonal expansion in response to a SARS-CoV-2 vaccine. We hypothesize that the profound reduction of Tfh cells in the Tfh deleter during primary vaccination results in substantially increased clonal competition for help, allowing only a few clones to dominate and expand, resulting in reduced diversity. Near-germline SARS-CoV-2 neutralizing antibodies have been found in both humans and mice. Some of these clones appear to be specific for SARS-CoV-2 Spike based on heavy chain sequence. Interestingly, although we found the lowest affinities for SARS-CoV-2 Spike in antibodies derived from GC B cells in Tfh-deleted mice, we also found some high-affinity clones with affinities comparable to those found in control mice.

The roles of Tfr cells in controlling GC clonal dynamics have been controversial (Sage and Sharpe, 2020). We previously showed that deletion of Tfr cells before GC formation results in increased GC B cells, leading to augmented antibody responses (including vaccine-specific and autoantibodies), but lower vaccine specific antibody affinity (Clement et al., 2019). Here we find that deletion of Tfr cells resulted in increased GC frequencies but diminished SARS-CoV-2 Spike-specific contribution in GCs, particularly for S1- and RBD-specific clones. We hypothesize that Tfr cells set high activation thresholds on GC B cells and the reduction in SARS-CoV-2 Spike-specific B cells in the GC during Tfr deletion is due to increased clonal competition of non-vaccine-specific clones. This contributes to the diminished frequency of SHM, possibly by eliminating the ability of B cells to test newly mutated BCRs. Interestingly, the decrease in SHM persisted during secondary vaccine responses even though Tfr cells were able to reconstitute by the time of secondary vaccination. This may be due in part to fewer mutated B cells emerging as memory cells during primary GCs that may enter secondary GCs later in Tfr-DTR mice.

Immunological aging is a complex process that includes multiple changes in the immune system, such as diminished naive lymphocyte repertoires, thymic involution, defective cytokine responses, and expansion of Treg cells (Frasca et al., 2020). Age-related defects in humoral immunity include expansion of fully suppressive Tfr cells as well as Tfh cell dysfunction (Sage et al., 2015). We found that during SARS-CoV-2 Spike protein vaccination, aged mice have substantial decreases in GC frequency and also substantially less RBD-specific antibody in serum. Surprisingly, despite the decrease in GC frequency, SARS-CoV-2 Spike-specific B cells were relatively able to participate in GCs. However, GC B cells in aging had alterations in SHM with a more diverse and bimodal distribution. This effect is likely due to the combined effects of Tfh and Tfr functions. For instance, the high activation threshold due to expanded Tfr cells and the lack of adequate Tfh probably help explain the abundance of germline sequences. However, it is likely that the low competition setting combined with high threshold for activation due to Tfr expansion may allow a very small number of clones to expand and mutate substantially.

Together, the results of this work demonstrate that GC clonal dynamics are highly complex, and both positive and negative

Figure 6. Early Tfh help optimizes somatic hypermutation during SARS-CoV-2 Spike protein vaccine boosting

(A) Schematic of experiment. Control (*Cd4*^{Cre} and *Cxcr5*^{wt}) or Tfh-DTR (*Cd4*^{Cre} *Cxcr5*^{LoxSTOPLoxDTR}) mice were vaccinated with an adjuvanted SARS-CoV-2 Spike protein vaccine and given DT until day 11. The mice received a SARS-CoV-2 vaccine boost on day 30 and draining lymph nodes were harvested on day 38.

(B) Assessment of total CD4$^+$PD-1$^+$CXCR5$^+$ follicular T (left), CD4$^+$PD-1$^+$CXCR5$^+$FoxP3$^-$ Tfh (middle), and CD4$^+$PD-1$^+$CXCR5$^+$FoxP3$^+$ Tfr (right) cells on day 38.

(C) Percentage of CD19$^+$GL7$^+$FAS$^+$ GC B cells out of all CD19$^+$ B cells.

(D) Serological analysis of SARS-CoV-2 Spike or RBD-specific IgG.

(E) Percentage of SARS-CoV-2 Spike-specific clones out of the total IgG$^+$ GC B cells from single-cell GC cultures (left). Number in the center of the circle plot indicates total number of IgG$^+$ GC B cells analyzed.

(F) Affinities of Spike-specific antibodies from single GC B cell cultures.

(G) BCR somatic hypermutation analysis for V-heavy (VH) chain in *ex vivo* sorted GC B cells, including analysis for singleton and expanded (found at least twice) clones using smoothing spline fitting of data.

(H) Analysis of clonal distribution from *ex vivo* GC B cells. Numbers indicate total number of clones and number of GC B cells analyzed. N75 index is represented on a per-mouse basis.

(I) Schematic of deletion during boosting experiment. Control (*Cd4*^{Cre} and *Cxcr5*^{wt}) or Tfh-DTR (*Cd4*^{Cre} *Cxcr5*^{LoxSTOPLoxDTR}) mice were vaccinated with a SARS-CoV-2 Spike protein vaccine and were boosted on day 30, followed by DT treatment. Draining lymph nodes were harvested on day 38.

(J) Spike- and RBD-specific IgG in serum from mice treated as in (I).

(K) Single GC B cell cultures from GC B cells as in (I). Numbers indicate total numbers of IgG$^+$ GC B cells analyzed. Data are from a single experiment and are representative of two independent repeats with n = 4–8 mice per group (A–C), are concatenated data from two independent experiments with n = 4–8 mice per group (D), are concatenated data from two independent experiments (E and F), are concatenated data from n = 3 mice per group from one representative experiment (G and H), or are concatenated data from two independent repeats with n = 4–6 mice per group (J and K). Student's two-tailed unpaired t test (A–D, J) or Mann-Whitney Test (G). ***$p < 0.001$, **$p < 0.01$, *$p < 0.05$. See also Figure S5.

signals by Tfh and Tfr cells, respectively, contribute to optimal GC reactions that balance affinity maturation and clonal diversity. It may be possible to fine-tune this balance to enhance vaccine responses, depending on whether highly mutated oligoclonal antibodies or less mutated highly diverse antibodies are beneficial.

Limitations of the study

One limitation may be that the deletion of Tfh and Tfr cells may not be complete. In addition, our inability to integrate expansion kinetics with epitope specificity and affinity limits the ability to separate entry from proliferation of GC B cells.

STAR★METHODS

Detailed methods are provided in the online version of this paper and include the following:

- KEY RESOURCES TABLE
- RESOURCE AVAILABILITY
  - Lead contact
  - Materials availability
  - Data and code availability
- EXPERIMENTAL MODEL AND SUBJECT DETAILS
  - Mice
- METHOD DETAILS
  - Vaccination
  - Flow cytometric analysis
  - Sorting
  - ELISA for antibody specificity in serum and culture supernatants
  - Single GC cell cultures
  - BCR-sequencing
  - Bio-layer interferometry
- QUANTIFICATION AND STATISTICAL ANALYSIS

SUPPLEMENTAL INFORMATION

Supplemental information can be found online at https://doi.org/10.1016/j.celrep.2022.110399.

ACKNOWLEDGMENTS

We thank Dr. Dan Barouch and the other members of the Massachusetts Consortium for Pathogen Readiness (Mass CPR) for helpful discussions. We thank Dr. Garnett Kelsoe for supplying the NB21 cell line. This work was made possible through grant support from the National Institutes of Health (R01AI153124, R01AI158413, R21AI158175) and the Merck Exploratory Science Center.

AUTHOR CONTRIBUTIONS

C.B.C., B.L.H., M.A.P., E.D.B., and R.L.C. performed experiments; H.Z., J.D., T.R-R., E.C.H., K.A.V., O.O.F., R.C.O., and D.J.H. provided key technical input and contributed to study design; C.B.C. and P.T.S. conceptualized the study, designed experiments, analyzed data, and wrote the manuscript. All authors reviewed the manuscript.

DECLARATION OF INTERESTS

T.R.R., E.C.H., K.A.V., O.O.F., R.C.O., and D.J.H. are employees of Merck & Co., Inc.

Received: July 26, 2021
Revised: November 18, 2021
Accepted: January 26, 2022
Published: February 1, 2022

REFERENCES

Alsoussi, W.B., Turner, J.S., Case, J.B., Zhao, H., Schmitz, A.J., Zhou, J.Q., Chen, R.E., Lei, T., Rizk, A.A., Mcintire, K.M., et al. (2020). A potently neutralizing antibody protects mice against SARS-CoV-2 infection. J. Immunol. *205*, 915–922.

Brochet, X., Lefranc, M.P., and Giudicelli, V. (2008). IMGT/V-QUEST: the highly customized and integrated system for IG and TR standardized V-J and V-D-J sequence analysis. Nucleic Acids Res. *36*, W503–W508.

Cavazzoni, C.B., Bozza, V.B.T., Lucas, T.C.V., Conde, L., Maia, B., Mesin, L., Schiepers, A., Ersching, J., Neris, R.L.S., Conde, J.N., et al. (2021). The immunodominant antibody response to Zika virus NS1 protein is characterized by cross-reactivity to self. J. Exp. Med., e20210580. https://doi.org/10.1084/jem.20210580.

Clement, R.L., Daccache, J., Mohammed, M.T., Diallo, A., Blazar, B.R., Kuchroo, V.K., Lovitch, S.B., Sharpe, A.H., and Sage, P.T. (2019). Follicular regulatory T cells control humoral and allergic immunity by restraining early B cell responses. Nat. Immunol. *20*, 1360–1371.

Crotty, S. (2019). T follicular helper cell biology: a decade of discovery and diseases. Immunity *50*, 1132–1148.

Ersching, J., Efeyan, A., Mesin, L., Jacobsen, J.T., Pasqual, G., Grabiner, B.C., Dominguez-Sola, D., Sabatini, D.M., and Victora, G.D. (2017). Germinal center selection and affinity maturation require dynamic regulation of mTORC1 kinase. Immunity *46*, 1045–1058 e6.

Fonseca, V.R., Ribeiro, F., and Graca, L. (2019). T follicular regulatory (Tfr) cells: dissecting the complexity of Tfr-cell compartments. Immunol. Rev. *288*, 112–127.

Frasca, D., Blomberg, B.B., Garcia, D., Keilich, S.R., and Haynes, L. (2020). Age-related factors that affect B cell responses to vaccination in mice and humans. Immunol. Rev. *296*, 142–154.

Fu, W., Liu, X., Lin, X., Feng, H., Sun, L., Li, S., Chen, H., Tang, H., Lu, L., Jin, W., and Dong, C. (2018). Deficiency in T follicular regulatory cells promotes autoimmunity. J. Exp. Med. *215*, 815–825.

Gitlin, A.D., Mayer, C.T., Oliveira, T.Y., Shulman, Z., Jones, M.J., Koren, A., and Nussenzweig, M.C. (2015). T cell help controls the speed of the cell cycle in germinal center B cells. Science *349*, 643–646.

Gong, F., Dai, Y., Zheng, T., Cheng, L., Zhao, D., Wang, H., Liu, M., Pei, H., Jin, T., Yu, D., and Zhou, P. (2020). Peripheral CD4+ T cell subsets and antibody response in COVID-19 convalescent individuals. J. Clin. Invest. *130*, 6588–6599.

Gonzalez-Figueroa, P., Roco, J.A., Papa, I., Nunez Villacis, L., Stanley, M., Linterman, M.A., Dent, A., Canete, P.F., and Vinuesa, C.G. (2021). Follicular regulatory T cells produce neuritin to regulate B cells. Cell *184*, 1775–1789.

Jacobsen, J.T., Hu, W., Tb, R.C., Solem, S., Galante, A., Lin, Z., Allon, S.J., Mesin, L., Bilate, A.M., Schiepers, A., et al. (2021). Expression of Foxp3 by T follicular helper cells in end-stage germinal centers. Science *373*, eabe5146.

Juno, J.A., Tan, H.X., Lee, W.S., Reynaldi, A., Kelly, H.G., Wragg, K., Esterbauer, R., Kent, H.E., Batten, C.J., Mordant, F.L., et al. (2020). Humoral and circulating follicular helper T cell responses in recovered patients with COVID-19. Nat. Med. *26*, 1428–1434.

Kaneko, N., Kuo, H.H., Boucau, J., Farmer, J.R., Allard-Chamard, H., Mahajan, V.S., Piechocka-Trocha, A., Lefteri, K., Osborn, M., Bals, J., et al. (2020). Loss of bcl-6-expressing T follicular helper cells and germinal centers in COVID-19. Cell *183*, 143–157.e13.

Kotlarz, D., Zietara, N., Milner, J.D., and Klein, C. (2014). Human IL-21 and IL-21R deficiencies: two novel entities of primary immunodeficiency. Curr. Opin. Pediatr. *26*, 704–712.

Kuraoka, M., Schmidt, A.G., Nojima, T., Feng, F., Watanabe, A., Kitamura, D., Harrison, S.C., Kepler, T.B., and Kelsoe, G. (2016). Complex antigens drive permissive clonal selection in germinal centers. Immunity *44*, 542–552.

Lefebvre, J.S., Masters, A.R., Hopkins, J.W., and Haynes, L. (2016). Age-related impairment of humoral response to influenza is associated with changes in antigen specific T follicular helper cell responses. Sci. Rep. *6*, 25051.

Lefranc, M.P., Giudicelli, V., Ginestoux, C., Jabado-Michaloud, J., Folch, G., Bellahcene, F., Wu, Y., Gemrot, E., Brochet, X., Lane, J., et al. (2009). IMGT, the international ImMunoGeneTics information system. Nucleic Acids Res. *37*, D1006–D1012.

Lu, Y., Jiang, R., Freyn, A.W., Wang, J., Strohmeier, S., Lederer, K., Locci, M., Zhao, H., Angeletti, D., O'connor, K.C., et al. (2021). CD4+ follicular regulatory T cells optimize the influenza virus-specific B cell response. J. Exp. Med. *218*, e20200547.

Masella, A.P., Bartram, A.K., Truszkowski, J.M., Brown, D.G., and Neufeld, J.D. (2012). PANDAseq: paired-end assembler for illumina sequences. BMC Bioinformatics *13*, 31.

Mcheyzer-Williams, M., Okitsu, S., Wang, N., and Mcheyzer-Williams, L. (2012). Molecular programming of B cell memory. Nat. Rev. Immunol. *12*, 24–34.

Mesin, L., Schiepers, A., Ersching, J., Barbulescu, A., Cavazzoni, C.B., Angelini, A., Okada, T., Kurosaki, T., and Victora, G.D. (2020). Restricted clonality and limited germinal center reentry characterize memory B cell reactivation by boosting. Cell *180*, 92–106 e11.

Mohammed, M.T., Cai, S., Hanson, B.L., Zhang, H., Clement, R.L., Daccache, J., Cavazzoni, C.B., Blazar, B.R., Alessandrini, A., Rennke, H.G., et al. (2021). Follicular T cells mediate donor specific antibody and rejection after solid organ transplantation. Am. J. Transpl. *21*, 1893–1901.

Retter, I., Althaus, H.H., Munch, R., and Muller, W. (2005). VBASE2, an integrative V gene database. Nucleic Acids Res. *33*, D671–D674.

Roco, J.A., Mesin, L., Binder, S.C., Nefzger, C., Gonzalez-Figueroa, P., Canete, P.F., Ellyard, J., Shen, Q., Robert, P.A., Cappello, J., et al. (2019). Class-switch recombination occurs infrequently in germinal centers. Immunity *51*, 337–350 e7.

Sage, P.T., and Sharpe, A.H. (2020). The multifaceted functions of follicular regulatory T cells. Curr. Opin. Immunol. *67*, 68–74.

Sage, P.T., Tan, C.L., Freeman, G.J., Haigis, M., and Sharpe, A.H. (2015). Defective TFH cell function and increased TFR cells contribute to defective antibody production in aging. Cell Rep. *12*, 163–171.

Tangye, S.G., Ma, C.S., Brink, R., and Deenick, E.K. (2013). The good, the bad and the ugly - TFH cells in human health and disease. Nat. Rev. Immunol. *13*, 412–426.

Tas, J.M., Mesin, L., Pasqual, G., Targ, S., Jacobsen, J.T., Mano, Y.M., Chen, C.S., Weill, J.C., Reynaud, C.A., Browne, E.P., et al. (2016). Visualizing antibody affinity maturation in germinal centers. Science *351*, 1048–1054.

Tiller, T., Busse, C.E., and Wardemann, H. (2009). Cloning and expression of murine Ig genes from single B cells. J. Immunol. Methods *350*, 183–193.

Victora, G.D., and Nussenzweig, M.C. (2012). Germinal centers. Annu. Rev. Immunol. *30*, 429–457.

Victora, G.D., Schwickert, T.A., Fooksman, D.R., Kamphorst, A.O., Meyer-Hermann, M., Dustin, M.L., and Nussenzweig, M.C. (2010). Germinal center dynamics revealed by multiphoton microscopy with a photoactivatable fluorescent reporter. Cell *143*, 592–605.

Webb, L.M.C., Fra-Bido, S., Innocentin, S., Matheson, L.S., Attaf, N., Bignon, A., Novarino, J., Fazilleau, N., and Linterman, M.A. (2021). Ageing promotes early T follicular helper cell differentiation by modulating expression of RBPJ. Aging Cell *20*, e13295.

Wing, J.B., Lim, E.L., and Sakaguchi, S. (2020). Control of foreign Ag-specific ab responses by Treg and Tfr. Immunol. Rev. *296*, 104–119.

Wu, H., Chen, Y., Liu, H., Xu, L.L., Teuscher, P., Wang, S., Lu, S., and Dent, A.L. (2016). Follicular regulatory T cells repress cytokine production by follicular helper T cells and optimize IgG responses in mice. Eur. J. Immunol. *46*, 1152–1161.

Ye, J., Ma, N., Madden, T.L., and Ostell, J.M. (2013). IgBLAST: an immunoglobulin variable domain sequence analysis tool. Nucleic Acids Res. *41*, W34–W40.

Yeh, C.H., Nojima, T., Kuraoka, M., and Kelsoe, G. (2018). Germinal center entry not selection of B cells is controlled by peptide-MHCII complex density. Nat. Commun. *9*, 928.

Zhang, J., Wu, Q., Liu, Z., Wang, Q., Wu, J., Hu, Y., Bai, T., Xie, T., Huang, M., Wu, T., et al. (2021). Spike-specific circulating T follicular helper cell and cross-neutralizing antibody responses in COVID-19-convalescent individuals. Nat. Microbiol. *6*, 51–58.

STAR★METHODS

KEY RESOURCES TABLE

REAGENT or RESOURCE	SOURCE	IDENTIFIER
Antibodies		
Anti-B220 (clone RA3-6B2) PE	BioLegend	RRID: AB_312992
Anti-CD19 (clone 6D5) APC/Cy7	BioLegend	RRID: AB_830706
Anti-CD4 (clone RM4-5) PerCP/Cy5.5	BioLegend	RRID: AB_893326
Anti-CD38 (clone 90) PacBlue	BioLegend	RRID: AB_10613289
Anti-CD95 (Jo2) PE/Cy7	BD Biosciences	RRID: AB_396768
Anti-Mouse T- and B-Cell Activation Antigen (clone GL-7) FITC	BD Pharmingen	RRID: AB_394981
Anti-CD138 APC	BioLegend	RRID: AB_10960141
Anti-CXCR5 (clone 2G8) Biotin	BD Biosciences	Cat# 551960
Anti-ICOS (clone 15F9) PE	BioLegend	RRID: AB_313335
Anti-PD-1 (clone RMP1-30) PE/Cy7	BioLegend	RRID: AB_572017
Anti-Foxp3 (clone FJK-16s) Alexa Fluor 488	eBiosciences	Cat# 53-5773-82
Mouse Anti-Ki-67 (clone B56) Alexa Fluor 647	BD Biosciences	Cat# 561126
Streptavidin BV421	BioLegend	Cat# 405225
Anti-mouse Ig UNLB	SouthernBiotech	RRID: AB_2794121
Anti-mouse IgG AP	SouthernBiotech	RRID: AB_2794293
SARS-CoV-2 (2019-nCoV) Spike Neutralizing Antibody	Sino Biological	RRID: AB_2857934
Chemicals, peptides, and recombinant proteins		
Diphtheria Toxin	Sigma-Aldrich	Cat# 322326
SARS-CoV-2 S protein, His Tag, Super stable trimer	ACROBiosystems	Cat# SPN-C52H9
SARS-CoV-2 (2019-nCoV) Spike S1-His Recombinant Protein (HPLC-verified)	Sino Biological	Cat# 40591-V08H
SARS-CoV-2 (2019-nCoV) Spike S2 ECD-His Recombinant Protein	Sino Biological	Cat# 40590-V08B
Recombinant Spike Protein RBD (His tag)	BEI Resources	Cat# NR-52306
Bovine Serum Albumin	Sigma-Aldrich	Cat# A3912
TCL Buffer	QIAGEN	Cat# 1031576
Addavax	Invivogen	Cat# vac-adx-10
Critical commercial assays		
MiSeq Reagent Nano Kit v2 (500-cycles)	Illumina	Cat#MS-103-1003
Agencourt RNAClean XP kit	Beckman Coulter	Cat#A63987
Anti-Mouse IgG Fc Capture (AMC) Biosensors	Sartorius	Cat#18-5088
RT maxima reverse transcriptase	Thermo Fisher Scientific	Cat# EP0753
Foxp3 / Transcription Factor Staining Buffer Set	eBioscience	Cat#00-5523-00
ANA-HEp2 Screen ELISA	Tecan	Cat# RE70151
Experimental models: Cell lines		
NB21.2D9	Kuraoka et al. (2016)	N/A
Experimental models: Organisms/strains		
Mouse: *Cd4*^{Cre} *Cxcr5*^{LoxSTOPLoxDTR}	Mohammed et al. (2021)	Tfh-DTR
Mouse: *Foxp3*$^{IRES\text{-}CreYFP}$ *Cxcr5*$^{IRES\text{-}LoxP\text{-}STOP\text{-}LoxP\text{-}DTR}$	Clement et al. (2019)	Tfr-DTR
Mouse: C57bl/6J	The Jackson Laboratory	N/A

(*Continued on next page*)

Continued

REAGENT or RESOURCE	SOURCE	IDENTIFIER
Oligonucleotides		
Barcoding primers	IDT	Mesin et al., 2020
Software and algorithms		
PandaSeq	Masella et al. (2012)	N/A
FASTX toolkit	http://hannonlab.cshl.edu/fastx_toolkit	N/A
IMGT database	Lefranc et al. (2009)	http://www.imgt.org/
Vbase2 database	Retter et al. (2005)	http://www.vbase2.org/
IgBLAST	Ye et al. (2013)	https://www.ncbi.nlm.nih.gov/igblast/
Prism software	Graphpad	RRID: SCR_002798
FlowJo software v10	Treestar	RRID: SCR_008520
Octet Data Analysis Software Version 10	https://www.sartorius.com/en/products/protein-analysis/octet-systems-software	N/A

RESOURCE AVAILABILITY

Lead contact

Further information and requests for resources and reagents should be directed to and will be fulfilled by the Lead Contact, Peter Sage (psage@bwh.harvard.edu).

Materials availability

The materials are listed in the key resources table, and are available from the Lead Contact.

Data and code availability

- All data reported in this paper will be shared by the lead contact upon reasonable request.
- This paper does not report original code.
- Any additional information required to reanalyze the data reported in this paper is available from the lead contact upon request.

EXPERIMENTAL MODEL AND SUBJECT DETAILS

Mice

C57bl/6J mice were from Jackson Laboratories. Tfh-DTR mice are defined as *Cd4*^{Cre} *Cxcr5*^{LoxSTOPLoxDTR} mice and have been published previously (Mohammed et al., 2021). *Cd4*^{Cre} *Cxcr5*^{wt} littermates were used as a control for Tfh-DTR mice. Tfr-DTR mice are defined as *Foxp3*$^{IRES\text{-}CreYFP}$ *Cxcr5*$^{IRES\text{-}LoxP\text{-}STOP\text{-}LoxP\text{-}DTR}$ mice and have been published previously (Clement et al., 2019; Mohammed et al., 2021). *Foxp3*$^{IRES-CreYFP}$ *Cxcr5*^{wt} littermates were used as a control for Tfr-DTR mice. Mouse progenies were routinely screened for leakiness of the *Foxp3*$^{IRES\text{-}CreYFP}$ allele by flow cytometry as described (Clement et al., 2019). Mice were males and females, 6-8 weeks old and aged mice were 80 weeks old. All mice were used according to Brigham and Women's Hospital Institutional Animal Care and Use Committee and National Institute of Health guidelines.

METHOD DETAILS

Vaccination

5μg of SARS-CoV-2 spike pre-fusion stabilized trimer (ACROBiosystems, SPN-C52H9) were combined 1:1 with Addavax adjuvant (Invivogen) and injected subcutaneously in the mouse flank. Vaccine boosting experiments were performed by injecting the same adjuvanted vaccine in the same flank location 30 days after primary vaccination. Mice received 0.5μg of diphtheria toxin i.p. at days 2, 5 and 8 post immunization to delete indicated cell types. To control effects of diphtheria toxin all mice received diphtheria toxin injections. Organs from mice were harvested on indicated timepoints.

Flow cytometric analysis

The following antibodies were used for surface staining at 4°C for 30 min: anti-CD4 (Biolegend, RM4-5), anti-ICOS (Biolegend, 15F9), anti-CD19 (Biolegend, 6D5), anti-PD-1 (Biolegend, RMP1-30), anti-CXCR5 biotin (BD Biosciences, 2G8), T- and B-cell activation antigen (BD Biosciences, GL-7), CD38 (Biolegend, 90), CD138 (Biolegend, 281-2), and anti-CD95 (BD Biosciences, Jo2),

Streptavidin-BV421 (Biolegend, 405225). For intracellular staining, samples were fixed with the Foxp3 Fix/Perm buffer set according to the manufacturers instructions (eBioscience). Samples were then intracellularly stained with anti-FoxP3 (eBiosciences, FJK-16S). No viability dye was included. Samples were analyzed on FACS Canto II (BD) or Cytek Aurora. Data was analyzed using FlowJo v10 (FlowJo LLC).

Sorting

Draining lymph nodes were passed through 70 micron filters and resuspended in PBS supplemented with 1% FBS and 1mM EDTA. Cells were stained with anti-B220 (Biolegend, RA3-6B2), CD38 (Biolegend, Clone 90), T- and B-cell activation antigen (BD Biosciences, GL-7), CD138 (Biolegend, 281-2), as well as anti-CD4 (Biolegend, RM4-5) for exclusion gate, for 30 minutes at 4°C. Cell sort was performed on a MoFlo Astrios instrument (Dako-Cytomation). GC B cells were defined as CD4- B220+ CD138- CD38lo/- GL-7+.

ELISA for antibody specificity in serum and culture supernatants

96-well plates (Nunc MaxiSorp, Thermo) were coated with 100 μL of SARS-CoV-2 Spike pre-fusion stabilized trimer (ACROBiosystems, SPN-C52H9) or SARS-CoV-2 Spike protein subunits (S1, S2 and RBD) at 2μg/mL, overnight at 4°C. Then, after 1h of blocking (PBS-1%BSA), 100 μL of diluted serum samples or culture supernatants were incubated for 1h at room temperature. 96-well half area plates (Microlon, Greiner) were used for supernatants. All volumes were reduced by half in this case. Serum dilution was 1:500 or 1:2,000 (for day 10 or 14 after vaccination) and 1:10,000 (for day 8 after boosting vaccination). Supernatants were not diluted. Standard curves were obtained by serial dilution of an RBD-specific monoclonal antibody (Sino Biological, 40591-MM43). Secondary antibody anti-mouse IgG conjugated to AP (Southern Biotech) was diluted 1:1,000 in PBS-BSA 1% and incubated for 1h at room temperature. Reactions were developed with AP substrate and absorbance was measured at 405 nm. Anti-nuclear antigen/HEp-2 cell-lysate ELISAs were performed using the ANA-HEp2 Screen ELISA kit (Tecan, RE70151), as described above.

Single GC cell cultures

Single GC B cells were sorted, as described above, into 96-well round-bottom plates (Corning) containing $1x10^3$ NB21.2D9 cells/well as previously described (Kuraoka et al., 2016; Cavazzoni et al., 2021) with minor modifications, such as not adding IL-4. Cells were cultured in OptiMEM (GIBCO) supplemented with 10% heat-inactivated fetal bovine serum (GIBCO, 16140071), 2 mM L-glutamine, 1 mM sodium pyruvate, 50 μM 2-mercaptoethanol, 100 U penicillin, and 100 μg/ml streptomycin. IgG secretion was assessed by ELISA after 6 days of culture and IgG+ supernatants were collected after 9 days of culture when cells were frozen in TCL lysis buffer supplemented with 1% 2-mercaptoethanol for *Igh* sequencing. One 96-well plate from each mouse was sorted. The frequency of Spike specific cells was calculated from the total of IgG+ wells. For the Spike specific frequency on a per mouse basis, only mice with at least 8 IgG+ wells were included.

BCR-sequencing

Germinal center B cells from draining lymph nodes were stained with anti-B220 (Biolegend, RA3-6B2), CD38 (Biolegend, Clone 90), T- and B-cell activation antigen (BD Biosciences, GL-7) CD138 (Biolegend, 281-2) and CD4 (Biolegend, RM4-5) for 30 minutes at 4°C in PBS with 1% FBS and 1mM EDTA. GC B cell population was defined as $B220^+$ $CD38^{lo/-}$ $GL\text{-}7^+$ $CD138^-$ $CD4^-$. Single cells were sorted into 96-well PCR plates containing 5 μl/well of TCL lysis buffer (Qiagen) with 1%β-mercaptoethanol for *Igh* sequencing. RNA extraction was performed using SPRI beads (Tas et al., 2016). RNA was reverse transcribed into cDNA using oligo (dT) primer. *Igh* transcripts were amplified (Tiller et al., 2009) and PCR products were barcoded and sequenced utilizing MiSeq (Illumina) Nano kit v.2, as previously described (Mesin et al., 2020). Paired-end sequences were assembled with PandaSeq (Masella et al., 2012) and processed using FASTX toolkit. *Igh* sequences were submitted to IMGT HighV-QUEST for V(D)J rearrangement assignment (Brochet et al., 2008). To identify VH mutations both IMGT (Lefranc et al., 2009) and Vbase2 (Retter et al., 2005) databases were used and, in case of discrepancy, IgBLAST (Ye et al., 2013)was used. VH mutation analyses were restricted to cells with productively rearranged *Igh* genes. Functional rearrangements were grouped into clones defined by same VH and JH segments, same CDR-H3 length and at least 80% similarity in CDR-H3 amino acid sequences.

Bio-layer interferometry

Bio-layer interferometry (BLI) was performed on an Octet RED96 instrument (ForteBio) to determine binding affinities of IgG from single GC B cell culture supernatants. Antibodies were immobilized in mouse Fc capture biosensors (Anti-Mouse IgG Fc Capture (AMC)). Association was measured by immersing biosensors loaded with IgG from culture supernatants in wells containing SARS-CoV-2 Spike recombinant trimer (75nM, 150nM, 300nM or 1μM in kinetics buffer provided by the manufacturer) for 600s. Dissociation was monitored after transfer of the biosensors into distinct wells containing kinetics buffer for 600s. K_D values are the ratio between the association (K_a) and dissociation (K_d) constants and were determined with the best concentration in which a local fit 1:1 binding indicated adequate goodness of fit (X^2 and R^2) both by the Octet data analysis software (ForteBio) and Prism 9 (GraphPad).

QUANTIFICATION AND STATISTICAL ANALYSIS

Statistical tests were performed using Prism 9 (GraphPad) utilizing Student's two-tailed unpaired t test for normalized data, or Mann Whitney test for non-normal data as indicated in figure legends. Frequency distributions of VH mutation numbers were plotted as curves utilizing smoothing splines with number of knots of 5. All measurements were taken from distinct samples, except for memory experiments in which the same mice were bled before and after boost.